Hindawi
Journal of Nanomaterials
Volume 2022, Article ID 5091110, 11 pages
https://doi.org/10.1155/2022/5091110

Research Article

Preparation of SnO_2-Based Composite Gas-Sensitive Material and Its Effect on the Membrane Treatment Process of Volatile Organic Compounds

Youping Shou, Junjie Zhao, and Jianzhe Qiao

Tianjin Research Institute for Water Transport Engineering, M.O.T., 300000 Tianjin, China

Correspondence should be addressed to Junjie Zhao; 631406010214@mails.cqjtu.edu.cn

Received 5 March 2022; Revised 18 June 2022; Accepted 4 July 2022; Published 2 August 2022

Academic Editor: Awais Ahmed

Semiconductor oxide-sensitive materials can be divided into n-type materials and p-type materials according to this characteristic. The carriers in n-type materials are mainly electrons, which are formed by the existence of a large number of oxygen vacancies in the material's crystal lattice. Common n-type materials include SnO_2, In_2O_3, and ZnO. This article is aimed at studying the effect of SnO_2-based composite gas-sensitive materials on the treatment process of volatile organic compounds. In this paper, the biomembrane method, the ultrafiltration membrane transmembrane pressure difference method, and the chemical reaction activity analysis method in the membrane treatment detection method are proposed, and then, the empirical kinetic model for the preparation of SnO_2-based composite gas-sensitive materials is established, and the TPU nanometer is analyzed. The cross-sectional scanning of the composite material explored the effect of the curing agent content on the SnO_2-based composite gas-sensitive material and analyzed the mechanical properties of the material. The experiment in this article uses 15 orders of magnitude of mechanics, which improves the scientific nature of the article. The experimental results show that the material modification has a better improvement effect on the film treatment process of volatile organic compounds.

1. Introduction

1.1. Background. With the development and progress of society, the population of urban areas has expanded, the flow of motor vehicles has increased, and chemical products have increased, but they have strong chemical activity. Some VOCs are also highly toxic and have certain hazards to the atmospheric environment and organisms. Affected by changes in the intensity of emission sources and traffic activities, VOCs exhibit regular daily and seasonal changes. The literature shows that there is a significant seasonal variation in the concentration of VOCs, which reaches the highest value in winter and drops to the lowest value in summer. Due to the low temperature in winter and the increase in coal consumption for heating, the increased VOC emissions increase the concentration level in the atmosphere, and the high temperature in summer reduces the consumption of coal and other energy sources. At the same time, high temperature promotes the elimination of some VOCs in the atmosphere and reduces the level. In addition, in the chemical plant area, VOCs are greatly affected by changes in temperature. Olefin compounds such as isoprene are mainly derived from the natural emissions of plants, and their changes show significant characteristics of plant emissions. However, none of these methods can fundamentally solve the volatility problem of volatile organic compounds such as styrene.

1.2. Significance. For the detection of harmful gases, there are currently two methods: large analytical instruments and gas sensors. Although large-scale analytical instruments have the advantages of accurate and high-precision gas detection, they cannot be the main method for gas detection due to their high price, inconvenience to carry, and inability to complete rapid detection. For more than half a century, through the continuous efforts of scientists, the application of semiconductor oxide sensors in real life has become more and more extensive. At the same time, the nanofiber

material has the advantages of uniform thickness and good morphology consistency, which reduces the influence of the morphology on the gas-sensing properties and facilitates the comparison of the gas-sensing properties of different materials. However, semiconductor gas sensors still have a series of problems such as inaccurate gas detection and poor accuracy. Therefore, it is necessary to develop high-performance gas sensors to complete the detection of the types and concentrations of harmful gases.

1.3. Related Work. Volatile organic compounds are an important air pollutant and have a huge destructive effect on the human living environment. Zheng et al.'s research is aimed at evaluating the efficiency of removing volatile organic compounds (VOC) from process gases in the eastern Polish food industry plant, which produces high-quality animals (geese, ducks, and pigs) and vegetable fats using two phases: method combined with biological purification and membrane separation. The research was conducted on a semitechnical scale and compared the effects of traditional and two-stage biological filtration under the same process conditions. The concentration of VOC in the process gas is measured by a multigas detector. In addition, the temperature and humidity of the gas are determined by a thermal anemometer under the filter bed, followed by two different types of filling materials (a mixture of stumps and bark, and a mixture of stumps, bark, and compost: European Union and Poland national standard methods) and two kinds of membranes (using three-layer semipermeable membrane fabrics with different air permeability and water tightness) were analyzed [1]. VOC (volatile organic compounds) are mainly produced in workplaces or laundry shops using spray paint processes or organic solvents. Large-scale plasma treatment of exhaust gas under industrial or municipal conditions requires a high-efficiency plasma conversion process at a high processing speed, that is, a large volume flow. Due to the use of plasma processing steps, the integration of the plasma unit into the existing system puts forward requirements for pipeline system compatibility and minimum pressure drop. The innovative rotating electrode sliding arc plasma device described in this article can meet these conditions. The system consists of propeller-shaped high-voltage electrodes in a grounded metal pipe. The design of the high-voltage electrode eliminates the pressure drop inside the air system. In contrast, the plasma device itself can drive exhaust gas with a tube diameter of 20 cm at a volume flow rate of up to 300 cubic meters per hour. They are composed of various forms of hydrocarbons. Because of their low concentration, they are diluted in the atmosphere, so it is difficult to burn directly with traditional burners. In this research, Sun et al. proposed a new form of VMDC (volume matrix dump) burner to process this low-calorie VOC gas. The burner configuration combines the characteristics of a plasma burner, dump burner, and volume matrix burner. Therefore, VMDC is configured to ensure sufficient decomposition temperature and residence time for stable flame formation and VOC decomposition. [2]. Although wood-based panels release harmful formaldehyde, they are still widely used. In order to protect humans from exposure to formaldehyde, we have successfully produced particle board by surface treatment of wood fibers and the use of unsaturated polyester resin (UP) as a formaldehyde-free binder. Phenolic (PF) aqueous solutions are used to treat wood particles to make them more compatible. Wan et al. inspected whether the mechanical properties of particleboard meet the national standard and M-1 level (ANSI A208.1-1999). The water absorption test confirmed the dimensional stability of FF particleboard. The performance of PF-treated FF particleboard is several times better than that of untreated FF particleboard. In addition, the effect of PF treatment on the adhesion of wood particles and UP interface was also studied by SEM, DMTA, and contact angle measurement. The results confirmed that PF treatment improved the interfacial adhesion between UP and wood particles [3]. Although his experimental studies have improved the interfacial adhesion between UP and wood particles, the adhesion is still insufficient.

1.4. Innovation. This paper introduces the curing kinetic parameter algorithm of unsaturated polyester resin, membrane processing detection method, chemical reaction activity analysis method, and other methods and then constructs the empirical kinetic model of unsaturated polyester resin, the preparation of cellulose nanocrystals, and study on the apparent kinetics of curing of unsaturated polyester resin and finally analyze the cross-sectional scan of the TPU nanocomposite, explore the effect of curing agent content on the gel time of unsaturated polyester resin, and analyze the mechanical properties of the material. According to the conclusions obtained after the comparison, the mechanism of the enhanced gas sensing properties of the composites and the mechanism of the conductivity type transition were analyzed.

2. Experimental Method

2.1. Gas Sensor Production. The experiment mainly uses hollow ceramic tubes to prepare indirectly heated gas sensors for gas sensitivity testing [4]. There are two ring electrodes in the middle of the ceramic tube, and each ring electrode leads out two pins. Put the metal oxide sensitive material prepared after the experiment into a mortar, add an appropriate amount of deionized water to it, and grind for 15-20 minutes, so that the sensitive material and deionized water are fully mixed to obtain a paste with good uniformity material [5, 6]. Use a brush to evenly coat the polished material on the middle part of the two electrodes of the ceramic tube, and the thickness should cover the electrodes. After drying at room temperature, put the coated ceramic tube in the muffle furnace, raise it to 300°C at a rate of 2°C/min, keep it for 120 minutes, and then lower it to room temperature at a rate of 3°C/min to ensure that the material is firmly attached to the electrode surface [7]. Pass the heating wire in the middle of the processed ceramic tube, weld the heating wire and the ceramic tube to the hexagonal base, aging in the air at a temperature of 300°C for 1 week, and then obtain a gas sensor that can be tested [8].

The static test system consists of air distribution box, DC power supply, A/D data acquisition card, and computer. The volume of the gas distribution box is 50 l, which is mainly used to prepare the required concentration of gas. The DC power supply is used to provide stable voltage, test voltage, and heating voltage for the gas sensor. The A/D data acquisition card (model USB7360B) is mainly used to convert the analog signal obtained by measuring the voltage of the sensitive element into a digital signal and then upload it to the computer for analysis by the software in the computer.

Since the VOC gas in this experiment is obtained through the vaporization of the corresponding organic solution, a heating crucible is equipped in the gas distribution box, which is to accelerate the evaporation of organic gas, and it is equipped with a gas exchange device and a test circuit [9]. During the test, the relationship between the volume V of the organic liquid to be injected and the gas concentration c in the gas distribution box is as shown in the formula:

$$\frac{p * w\% * v}{M} = \frac{V * c}{22.4 * (273 + T)/273}. \quad (1)$$

After simplification, you can get

$$v = \frac{V * c * M * 273}{(273 + T) * 22.4 * p * w\%}. \quad (2)$$

In the formula, M represents the molar mass of the gas to be tested, p represents the density of the organic liquid, $w\%$ represents the mass fraction of the component to be tested in the organic liquid, V represents the volume of the test chamber, and T is the temperature of the test chamber. For p-type materials, the expression of the response value S of the gas

$$S = \frac{Rg}{Ra} = \frac{Ug(10 - Ua)}{Ua(10 - Ug)}. \quad (3)$$

For n-type materials, the gas response value S can be expressed as

$$S = \frac{Ra}{Rg} = \frac{Ua(10 - Ug)}{Ug(10 - Ua)}. \quad (4)$$

In the formula, Ua and Ug are the voltage values of the tested component measured by the static test system in air and organic gas, respectively.

2.2. Membrane Treatment and Detection Method

2.2.1. Ultrafiltration Membrane Transmembrane Pressure Difference Method. The experiment uses the change of transmembrane pressure difference as the basis for evaluating the fouling rate of the ultrafiltration membrane, and the transmembrane pressure difference is monitored online by a pressure gauge [10]. The detected water quality data includes the turbidity, SDI, and CODMn of the incoming and outgoing water of each processing unit. The surface morphology changes of ultrafiltration membranes under different operation modes are analyzed.

In order to explore the pollution mechanism of ultrafiltration under different pretreatment conditions, the experiment refers to the Darcy resistance model [11] and analyzes each part of the resistance generated during the ultrafiltration process. The formula is as follows:

$$J = \frac{\Delta p}{\mu(R_m + R_f + R_c)} = \frac{\Delta p}{\mu R_t}. \quad (5)$$

Each resistance can be calculated by the following formula:

$$R_m = \frac{\Delta p}{\mu j_{iw}}, \quad (6)$$

$$R_f = \frac{\Delta p}{\mu j_{iw}} - R_m, \quad (7)$$

$$R_c = \frac{\Delta p}{\mu j} - (R_m + R_f), \quad (8)$$

where j_{iw} is the initial membrane water flux, $m^3/(m^2 \cdot h)$ and j is the membrane water flux after pollution, $m^3/(m^2 \cdot h)$.

Membrane treatment ultrafiltration technology has broad prospects in the treatment of volatile gases, sewage, drinking water, and surface water due to its own advantages. Based on the current problems of ultrafiltration, this research studies the pollution mechanism of ultrafiltration membranes to alleviate membrane pollution and reduce the cost of ultrafiltration. It also compares and analyzes the current commonly used pretreatment methods to find out suitable pretreatment methods such as Figure 1 shows the ultrafiltration device and its simple schematic diagram.

2.3. Chemical Reaction Activity Analysis Method. Although the content of VOCs in the atmosphere is small, they can undergo a series of chemical reactions with oxidants such as OH radicals, HO_2 radicals, and O_3 in the atmosphere and play an important role in the elimination of atmospheric oxidants, thereby affecting the global OH radicals Distribution. On the other hand, VOCs can interact with NOx in the atmosphere and have an important impact on the formation of tropospheric ozone on a regional or even global scale. VOCs and ozone and other photochemical oxidation products can endanger the health of exposed people. VOCs have high volatility and also have characteristics such as permeability and lipophilicity. Most of the aromatic compounds are toxic and harmful substances. Due to the high lipophilicity, these compounds will enter the human body through respiration and be enriched. People who are exposed to these low-concentration toxic and harmful pollutants for a long time will produce chronic hazards. This hazard is often difficult to attract people's attention. These pollutants mainly irritate the eyes and nasal mucosa through contact with the respiratory mucosa, resulting in chronic bronchitis and asthma. Physiological dysfunctions such as lung cancer and

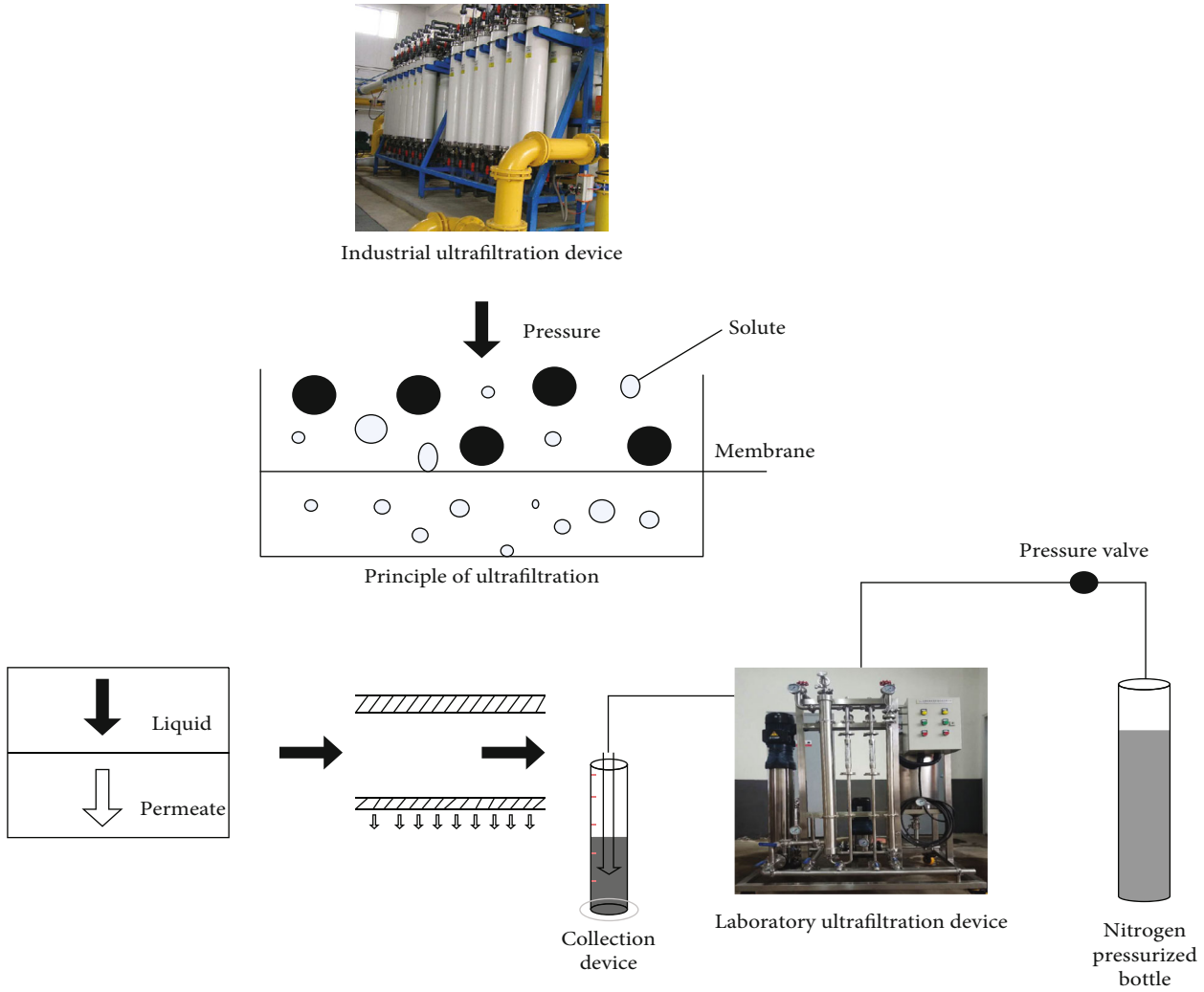

Figure 1: Ultrafiltration experimental device and principle.

lung cancer aggravate the condition of hypertension and heart disease.

At present, there are two main methods used to measure the reactivity of VOCs and their contribution to ozone production: First, the reactivity of VOCs species is expressed as

$$L_i^{\mathrm{OH}} = [\mathrm{VOCs}]_i \times K_i^{\mathrm{OH}}. \tag{9}$$

Calculate the reactivity of each component of VOCs and then add the LiOH of each species in the component:

$$L^{\mathrm{OH}} = \sum [\mathrm{VOCs}]_i \times K_i^{\mathrm{OH}}, \tag{10}$$

$$\Phi_{\mathrm{ofp}} = \xi_{\mathrm{MIR}} \times \rho(c_2 - c_{12}). \tag{11}$$

2.4. Performance Indicators of Gas Sensors. The performance of the gas sensor is mainly judged by the following aspects: the response value of the gas sensor, the working temperature, the selectivity, the response-recovery time, the stability, etc.

The response of the gas sensor to the gas to be measured will be affected by temperature, because the gas to be measured requires a certain amount of energy to react on the surface of the gas sensor [12, 13]. When the temperature is too low, the energy provided is too little, which will result in too little gas to be measured on the surface of the sensor, resulting in a relatively low response value; when the temperature is too high, it will lead to waste of energy and even damage to the device [14]. At a specific temperature, the sensitive element will show the maximum response value of the gas to be measured, and this temperature is usually called the optimal working temperature of the element. A lower optimal working temperature or even room temperature operation is one of the necessary conditions for a sensor with good performance [15, 16].

Selectivity is obtained by comparing the response value of the sensor to a specific gas with the response value of other gases [17]. It is known that the sensitive element will respond to a variety of gases when working at the optimal operating temperature, which will cause errors in the measurement. Therefore, it is necessary to prepare components with good selectivity.

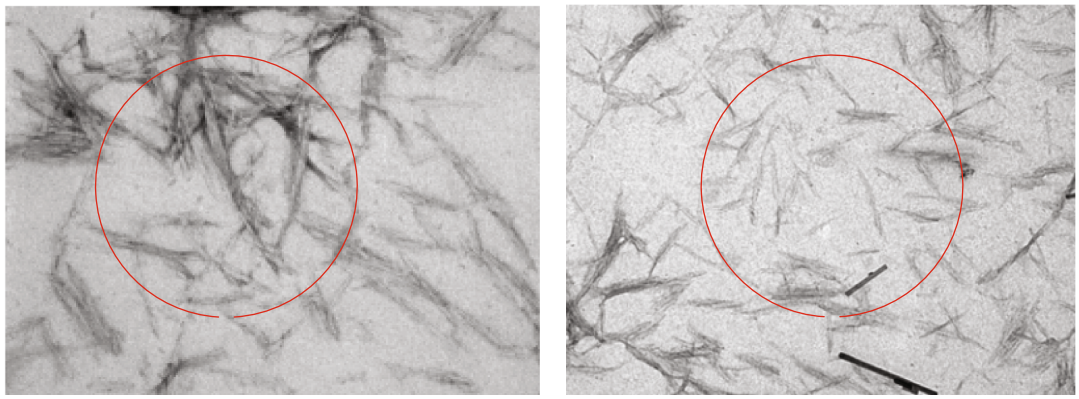

(a) (b)

Figure 2: Transmission electron microscopy (TEM) photo of cellulose nanocrystals (a) 70,000 times magnification and (b) 40,000 times magnification.

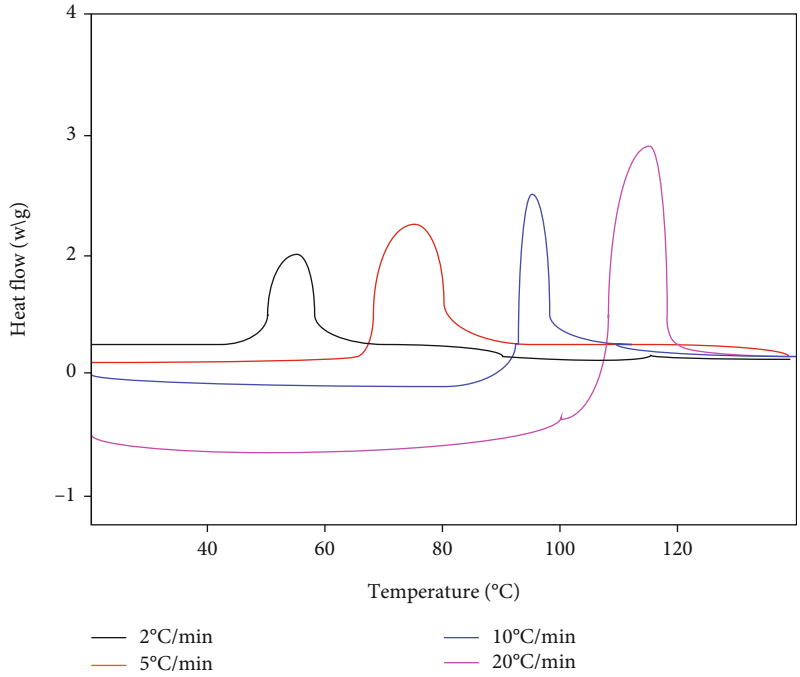

Figure 3: DSC curves of composite gas-sensitive materials at different heating rates.

Table 1: Characteristic temperature of DSC curve (°C).

B (°C/min)	Ti (°C)	Tp (°C)	Tf (°C)
2	46.8	54.5	62.5
5	65.1	73.1	81.2
10	76.9	91.0	107.2
20	82.6	100.8	125.7

Table 2: Composite gas-sensitive material curing kinetics data.

B (°C/min)	Tp (°C)	Tp (K)	$1/Tp$	$-\ln \beta/T^2_p$	$\ln \beta$
2	54.5	327.6	$3.053 * 10^{-3}$	10.890	0.693
5	73.1	346.3	$2.888 * 10^{-3}$	10.085	1.609
10	91.0	364.2	$2.746 * 10^{-3}$	9.493	2.303
20	100.8	374.0	$2.671 * 10^{-3}$	8.853	2.996

When it comes into contact with the gas to be measured, it takes a certain time for the sensitive element to reach the maximum response value [18]. The time when the initial state reaches 90% of the maximum response value is usually defined as the response time; similarly, when it is separated from the gas to be measured, the sensitive element needs to be restored. It takes a certain time to restore to the original state. Usually, the time from the maximum response value to 10% of the maximum response value is defined as the recovery time. Shortening the response-recovery time is helpful for continuous detection, so the response-recovery time is also an important parameter of the gas sensor.

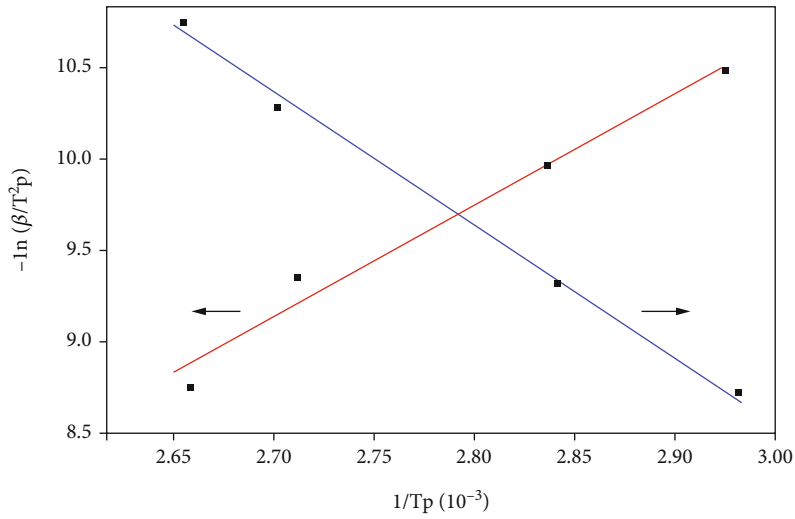

Figure 4: $\ln(\beta/T^2_p) \sim 1/Tp$ and $\ln \beta \sim 1/Tp$ of the curing reaction of composite gas-sensitive materials.

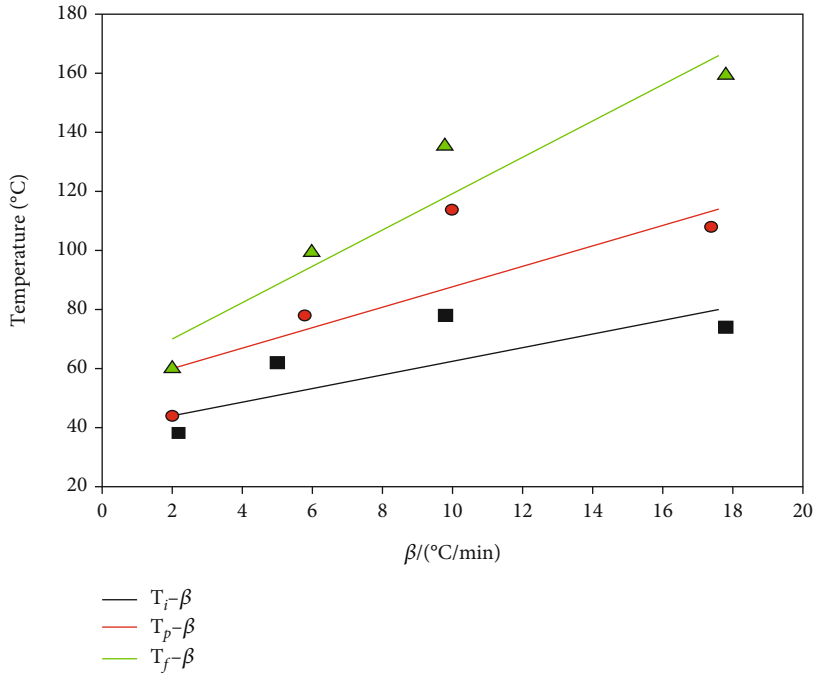

Figure 5: The relationship between T and β.

If the gas sensor is used for a long time or stored for a long time, its internal structure will change, causing the resistance to drift when measuring gas [19]. This will cause problems such as a decrease in the response value, which will affect the accuracy of the measurement. Therefore, stability is the decisive factor for whether the gas sensor can be applied in real life. The performance of these sensors is mainly determined by the characteristics of sensitive materials. Therefore, in order to make a gas sensor with good performance, it is necessary to prepare a sensitive material with good characteristics.

For gas sensors, sensitive materials with good characteristics must be prepared. The gas-sensing characteristics of sensitive materials are mainly determined by factors such as the composition of the material, the morphology of the material, the porosity of the material, the size of the grain size of the material, and the specific surface area of the material. Therefore, improving the gas-sensing properties of sensitive materials can be achieved through physical modification and chemical modification.

3. Experimental Inquiry

3.1. Establishment of an Empirical Kinetic Model of Unsaturated Polyester Resin. The curing kinetics of unsaturated polyester resins can be roughly divided into two

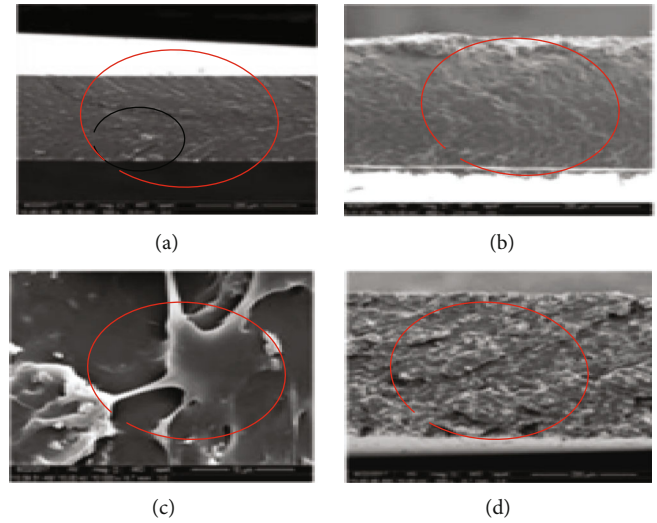

Figure 6: (a) GO/TPU, (b) GOE/TPU, (c) GOS/TPU, and (d) cross-sectional SEM image.

categories: empirical kinetic models and mechanism kinetic models [20]. The former does not consider the specific reaction process between the reactants, but a curing kinetic model equation established by mathematical simulation of a series of kinetic parameters measured through experiments during the curing reaction process. The latter is a curing kinetic model based on the principle of free radical polymerization. Unsaturated polyester resins include chain initiation, chain extension, and chain termination during the curing process, which are related to each other, and the reaction is difficult to stay in a certain way. In the first stage, with many parameters, it is difficult to get a suitable model. Therefore, empirical kinetic models are more commonly used to analyze the curing kinetics of unsaturated polyester resins.

The kinetic model of the n-order reaction model of unsaturated polyester resin is expressed as

$$\frac{d_a}{d_t} = kn(1-a)^n. \tag{12}$$

Curing reaction rate equation:

$$\frac{d_a}{d_t} = \mathrm{An}(1-a)^n \exp\left[-\frac{E}{\mathrm{RT}}\right]. \tag{13}$$

The expression of the autocatalytic model is

$$\frac{d_a}{d_t} = (_1 + k_2 a^m)(1-a)^n, \tag{14}$$

where k_1 is the reaction rate constant when $t = 0$ and k_2 is the reaction rate constant when $t > 0$, and both conform to the Arrheriu formula. m and n are the reaction order. Generally, it is assumed that the reaction order is 2 (i.e., $m + n = 2$). Equation (14) is widely used to describe the autocatalytic model of isothermal curing behavior of epoxy resin; afterwards, Ahmed et al. [21] did further research on Equation (14) and found that when $k_1 = 0$, it can be better used to study the isothermal curing kinetics of unsaturated polyester resin; the equation is as follows:

$$\frac{d_a}{d_t} = k_2 a^m (1-a)^n. \tag{15}$$

For this equation, there are also many application examples. Researchers have studied the curing kinetics of unsaturated polyester resin/composite initiation system and BMC materials and found that the selection of Equations (9)–(15) can well describe the curing reaction of unsaturated polyester resin.

3.2. Preparation of Cellulose Nanocrystals

3.2.1. Extraction of Cellulose Nanocrystals. According to related literature, cellulose nanocrystals (CNs) are extracted from cotton linters by sulfuric acid acidolysis. The specific steps are as follows: disperse 20 g of cotton linters in 175 ml with a concentration of 30% (v/v) sulfuric acid solution. The stirring was continued for 6 hours at a speed of 100 rpm at 60°C. After the reaction, the residual sulfonic acid groups on the surface of CNs were removed. Finally, freeze-dry at a low temperature of -50°C for more than 3 days. The CNs from which the distilled water has been removed are ground to obtain a white powder.

3.2.2. The Acetylation Process of Cellulose Nanocrystals. Weigh 5 g of CNs in 100 ml of anhydrous pyridine to ultrasonically disperse for 15 min to obtain a CNs suspension. Place it in a three-necked flask. Then, prepare a mixed solution of 25 ml of acetic anhydride and 20 ml of anhydrous pyridine. Add the acetic anhydride pyridine solution dropwise to the CN pyridine suspension through a separatory funnel to carry out the acetylation reaction. The acetylation process is carried out in a three-necked flask by condensing reflux. React at 400 rpm for 5 h at °C. After the reaction, the product in the three-necked flask was poured into 1 l of

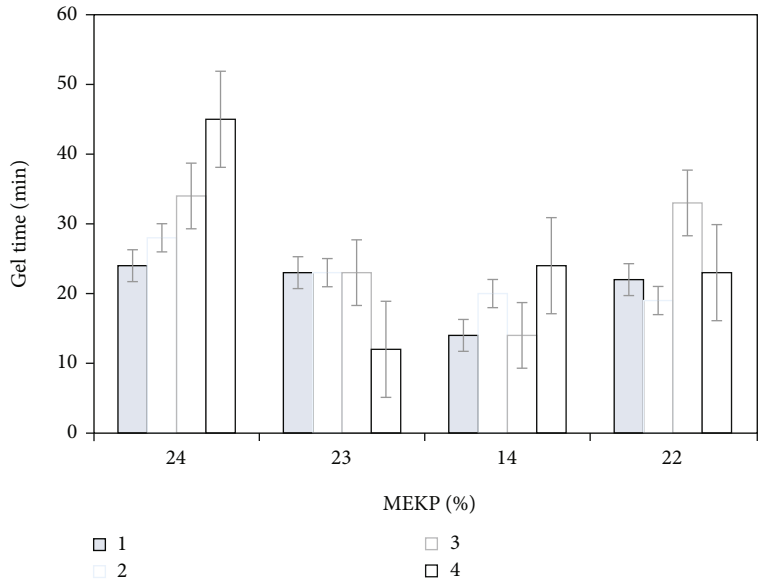

Figure 7: The effect of the amount of curing agent on the time of the composite gas-sensitive material was studied.

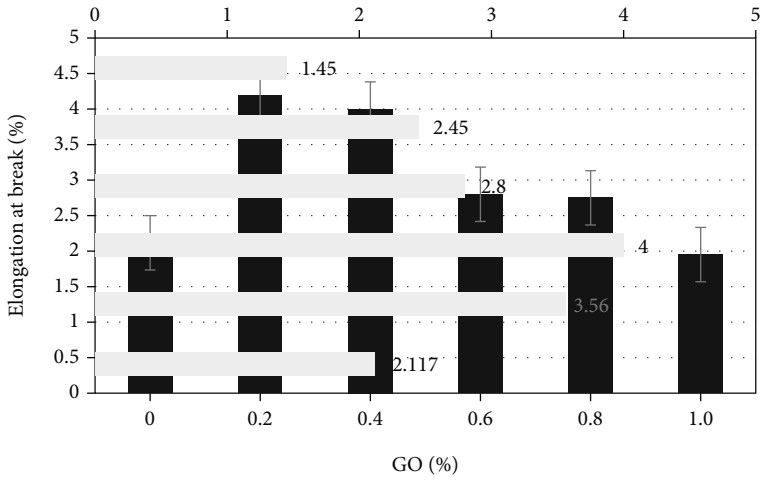

Figure 8: Comparison of elongation at break of graphene oxide/hydroxylated carbon nanotubes synergistically modified composite gas-sensitive materials.

Table 3: Mechanical properties of the composites.

Sample	Tensile strength (MPa)	Flexural modulus of elasticity (MPa)	Elongation at break (%)
0	38.42	2020.95	2.117
0.1	57.05	1678.46	4.189
0.25	53.31	1547.16	3.983
0.5	44.68	1721.01	2.896
0.75	45.96	1843.57	2.774
1	34.69	1931.86	1.951

distilled water to terminate the reaction, and the cellulose nanocrystals were precipitated, washed three times with acetone centrifugal precipitation, and then washed three times with distilled water. Then, it was dialyzed in distilled water for 12 hours, and finally, the acetylated cellulose nanocrystals were freeze-dried, and the freeze-dried acetylated cellulose nanocrystals were ground to obtain a white powdery product (ACN).

Figure 2 shows a transmission electron microscopy (TEM) image of cellulose nanocrystals (CNs), using sulfuric acid hydrolysis to remove the amorphous areas in the linters cellulose and successfully extract CNs. After observation, the extracted CNs have a rod-like nanomorphology structure. The length of CNs was measured with the Image-Pro software to measure the average size length: length $L = 310.1 \pm 47.8$ nm and width $D = 18.9 \pm 6.2$ nm.

3.3. Study on the Apparent Kinetics of Curing of Unsaturated Polyester Resin. When using the DSC method to solve the curing kinetic parameters of the SnO_2-based composite

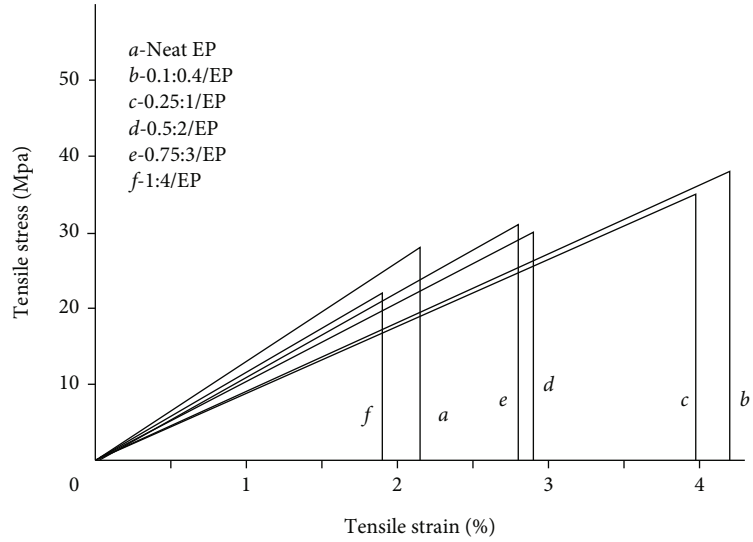

Figure 9: Stress-strain curve of graphene oxide/hydroxylated carbon nanotubes synergistically modified composite gas-sensitive material.

gas-sensitive material, it is necessary to test the DSC curves at different heating rates. The test result is shown in Figure 3.

In order to study the curing reaction kinetics of SnO_2-based composite gas-sensitive materials, it is necessary to solve the kinetic parameters such as the apparent activation energy (E) and reaction order (n) of the gas-sensitive materials and use the curing kinetic equation to describe the parameters and curing conditions. Table 1 shows the characteristic temperature (°C) of the DSC curve. Table 2 shows the curing kinetics data of the gas-sensitive material.

As shown in Figure 4, in order to achieve the above goal, linear fitting of the above known points can be obtained: $-\ln \beta/T^2{}_P \sim 1/Tp$ has a slope of $5.111 * 10^3$ and an intercept of -4.683, then $E/R = 5.111 * 10^3$, $\ln(AR/E) = 4.683$, so that the activation energy of DHEM50-1 resin system $E = 42.48$ kJ/mol, frequency factor $A = 5.523 * 10^5$. By linear fitting, it can be known that the slope of $\ln \beta \sim 1/Tp$ is $-5.81 * 10^3$, then $E/nR = 5.81 * 10^3$, since E has been obtained, substituting can be obtained $n = 0.880$.

Using the DSC method to solve the kinetics of composite gas-sensitive materials , the curing characteristic temperature of composite gas-sensitive materials can be preliminarily estimated. The relationship between temperature T and heating rate β is $T = C + B\beta$ (°C).

Use T-β to plot and get three different straight lines through linear fitting. As shown in Figure 5, when $\beta = 0$, the temperature of the composite gas-sensitive material is 51.5°C, the curing temperature is 57.8°C, and the postcuring temperature is 62.8°C. The above experiment test has no other fillers, and the dosage is small. Therefore, in actual production, it needs to be adjusted according to different situations.

4. Material Performance Analysis

4.1. Sectional Scanning Analysis of TPU Nanocomposite. The fracture surface morphology of TPU and its composites was analyzed. Figure 6 shows the fracture SEM images of GO/TPU, GOE/TPU, GOS/TPU, and GOES/TPU composites with a filler content of 2 wt%. From Figures 6(a) to 6(d), it can be seen to varying degrees that the fracture surface has begun to become rough, with wrinkles and gullies appearing, which indicates that there is a strong interface interaction between the nanoparticles and the matrix. In addition, the composite material in Figure 6(d) is the roughest, and it is magnified to observe that GOES nanoparticles prepared by the stitching effect of EDA and SiO2 coating can effectively improve the mechanical properties of TPU. This shows that this unique stitched and multisize graphene-based material helps to enhance the interface interaction between the filler and the matrix.

4.2. The Effect of Curing Agent Content on the Time of Composite Gas-Sensitive Materials. Figure 7 shows the effect of curing agent content on the time of the composite gas-sensitive material. It can be seen from Figure 7 that when the composition ratio, temperature, and other conditions of the composite gas-sensitive material remain unchanged, with the increase of the initiator MEKP and the accelerator TZ-9, the time of the composite gas-sensitive material gradually shortens, and the time decreases gradually. This is because the amount of initiator methyl ethyl ketone peroxide added is greater than the amount of accelerator cobalt salt added, so the greater the amount of initiator added, the more initial free radicals generated per unit time of methyl ethyl ketone peroxide, and the increase of initial free radicals can be accelerated resin free radical reactions; these reactions are exothermic reactions, which will increase the temperature of the system and accelerate the reaction rate again; however, the reaction rate of the composite gas-sensitive material cannot be increased indefinitely. This is mainly because the content of double bonds in the composite gas-sensitive material is limited, and these double bonds can only react with a limited number of free radicals. Therefore, when the initiator content increases again, the

composite gas-sensitive material time will be shortened, but the downward trend will decrease. When the initiator MEKP in the DHEM50-1 composite gas-sensitive material is added in the amount of 0.8-2 wt%, the time of the DHEM50-1 composite gas-sensitive material is in the range of 19-28 min.

4.3. Mechanical Properties. As shown in Figure 8 in conjunction with Table 3, the elongation at break and tensile strength of the material first increase and then decrease.

Figure 9 shows the tensile strength curve of GO-MWCNTs/EP material. Combined with the data in Table 3, it can be seen.

As shown in Figure 9, on the other hand, in the GO/EP system, when the GO content is 0.25 wt%, the mechanical properties of the material are the best, while in the GO-MWCNTs/EP system, when our GO content is reduced from 0.25 wt%. When it reaches 0.1 wt%, it can be seen from the graph that MWCNTs decreases with the decrease of GO content. The above experiments all show that the content of GO will enhance the material to a certain extent and is beneficial to the performance of the material.

5. Conclusions

The environmental effects of volatile organic compounds in the atmosphere are mainly manifested in their strong chemical activity. These active substances can participate in atmospheric chemical reactions, change the chemical properties of the atmosphere, and then change the air quality. This article mainly discusses the influence of composite gas-sensitive materials on the treatment process of volatile organic compounds exhaust gas membrane. It is hoped that effective treatment methods can be explored to reduce the emission and absorption of volatile organic compounds, so as to achieve the purpose of protecting the environment and improving human health. The double bond of the composite gas-sensitive material can undergo free radical polymerization with the double bond in the double bond monomer molecule as the crosslinking component under light conditions and form a more complex three-dimensional network structure under thermal initiation conditions. Combination of volatile organic compounds reduces pollution emissions. However, as far as the current situation is concerned, the technology is not perfect enough, and further research and development are needed. There are many ways to improve the gas sensing properties. The influence of the composite materials formed by doping on the gas sensing mechanism is relatively complicated. The relationship between the heterostructures composed of different materials and the gas sensing properties needs to be further studied.

Data Availability

No data were used to support this study.

Conflicts of Interest

The authors declare that they have no conflicts of interest.

Acknowledgments

This work was supported by the Research and development of safe and efficient treatment technology and equipment for shipping waste gas of highly toxic hazardous chemicals (TKS20210204).

References

[1] Z. Zheng, M. C. Cox, and B. Li, "Surface modification of hexagonal boron nitride nanomaterials: a review," *Journal of Materials ence*, vol. 53, no. 1, pp. 66–99, 2018.

[2] M. Sun, J. Ma, Y. Zeng, and Z. Liu, "Surface modification-the booster for application of magnetic nanomaterials," *Gongneng Cailiao/Journal of Functional Materials*, vol. 49, no. 4, pp. 04032–04039, 2018.

[3] E. Wan, L. Y. Heng, and M. Arip, "Surface modification of cellulose nanomaterial for urea biosensor application," *Sains Malaysiana*, vol. 47, no. 5, pp. 941–949, 2018.

[4] Z. Xiong, M. Shen, and X. Shi, "Zwitterionic modification of nanomaterials for improved diagnosis of cancer cells," *Bioconjugate Chemistry*, vol. 30, no. 10, pp. 2519–2527, 2019.

[5] O. V. Chudina, A. V. Eletskii, E. V. Terent'ev, and G. S. Bocharov, "Steel surface modification with carbon nanomaterial using concentrated energy flows," *Metal Science and Heat Treatment*, vol. 60, no. 5-6, pp. 367–372, 2018.

[6] Y. Niu and W. Hong, "Dielectric nanomaterials for power energy storage: surface modification and characterization," *ACS Applied Nano Materials*, vol. 2, no. 2, pp. 627–642, 2019.

[7] L. A. Urkhanova, S. A. Lkhasaranov, and S. L. Buyantuev, "Modification of cement and concrete with carbon nanomaterials, obtained by plasma method," *International Journal of Civil Engineering and Technology*, vol. 9, no. 1, pp. 652–656, 2018.

[8] N. P. Dikiy, A. N. Dovbnya, Y. V. Lyashko, E. P. Medvedeva, D. V. Medvedev, and I. D. Fedorets, "Modification of nanomaterial by radiation," *Problems of Atomic Science and Technology*, vol. 105, no. 5, pp. 83–87, 2016.

[9] X. Xu, Q. Zhou, N. Song, Q. Ni, and L. Ni, "Kinetic analysis of isothermal curing of unsaturated polyester resin catalyzed with tert-butyl peroxybenzoate and cobalt octoate by differential scanning calorimetry," *Journal of Thermal Analysis and Calorimetry*, vol. 129, no. 2, pp. 843–850, 2017.

[10] F. Tong and H. Ding, "numerical simulation and experiment of hardening behaviors in unsaturated polyester resin artificial marble blocks under microwave radiation," *IEEE Transactions on Plasma Science*, vol. 44, no. 10, pp. 2485–2492, 2016.

[11] Z. H. Dai, Q. Li, Z. W. Chen et al., "Reactive diluent derived from ferulic acid for the preparation of a fully biobased unsaturated polyester resin," *ACS Sustainable Chemistry & Engineering*, vol. 8, no. 47, pp. 17379–17386, 2020.

[12] G. W. Lee, K. Kim, C. J. Yoon, S. Yoon, and J. H. Choi, "Development of braille block for visually-impaired persons using unsaturated polyester resin," *Materials Today: Proceedings*, vol. 3, no. 2, pp. 99–103, 2016.

[13] M. Barcikowski, W. Krolikowski, and S. Lenart, "Microstructures of unsaturated polyester resins modified with reactive liquid rubbers," *Polimery*, vol. 62, no. 9, pp. 650–657, 2017.

[14] A. N. Johari, M. R. Ishak, Z. Leman, M. Z. M. Yusoff, and M. R. M. Asyraf, "Influence of CaCO3 in pultruded glass fiber/unsaturated polyester resin composite on flexural creep behavior

using conventional and time-temperature superposition principle methods," *Polimery*, vol. 65, no. 11-12, pp. 46–54, 2020.

[15] E. E. Al-Obeidi, M. M. Uonis, and M. A. Al-Jubouri, "Leverage of cigarette ash powder concentrations on the alternating bending fatigue of unsaturated polyester resin," *International Journal of Advanced Research*, vol. 8, no. 11, pp. 675–682, 2020.

[16] M. Farsane, L. Soufia, A. Anouar, S. Chah, S. Dagdag, and M. Bouzziri, "Experimental evaluation of the curing of unsaturated polyester resin at various amounts of methyl ethyl ketone peroxide, cobalt octoate and porcelain powder," *Revista de Chimie-Bucharest-Original Edition*, vol. 71, no. 10, pp. 58–66, 2020.

[17] V. Geaman, M. A. Pop, I. Radomir, A. Semenescu, B. Florea, and O. R. Chivu, "The influence of thermal behaviour to composites based on cotton tissue and unsaturated polyester resin," *Materiale Plastice*, vol. 57, no. 1, pp. 197–201, 2020.

[18] C. E. Odoala, I. O. Igwe, S. N. Okonkwo, and I. P. Oragwu, "Evaluation of mechanical properties of unsaturated polyester resin composite tiles of granite quarry dust filler," *International Journal of Scientific and Engineering Research*, vol. 11, no. 7, pp. 1737–1745, 2020.

[19] P. Wang, T. Yao, Z. Li et al., "A superhydrophobic/electrothermal synergistically anti-icing strategy based on graphene composite," *Composites Science and Technology*, vol. 198, p. 108307, 2020.

[20] N. Martin, F. Smarandache, and S. Broumi, "PROMTHEE plithogenic Pythagorean hypergraphic approach in smart materials selection," *International Journal of Neutrosophic Science*, vol. 13, no. 1, pp. 52–60, 2021.

[21] A. A. Elngar and S. I. El-Dek, "Novel artificial face mask based nanofibers with special intelligent engineered nanocomposite against Covid-19," *Journal of Cybersecurity and Information Management*, vol. 5, no. 2, pp. 21-22, 2020.